J. Phys. Chem. A **2007,** *111,* 13075−13087

Bonding Analyses, Formation Energies, and Vibrational Properties of M−R_2dtc Complexes (M = Ag(I), Ni(II), Cu(II), or Zn(II))

I. Georgieva* and N. Trendafilova

Institute of General and Inorganic Chemistry, Bulgarian Academy of Sciences, Sofia, Bulgaria

Received: June 27, 2007; In Final Form: September 12, 2007

Detailed theoretical studies based on density functional theory (DFT)/B3LYP calculations of dimethyl- and diethyldithiocarbamate complexes of Ni(II), Cu(II), Zn(II), and Ag(I) are performed to characterize the metal−ligand bonding type as well as the metal−ligand bonding strength depending on the metal and the dialkyl substituent. The metal−ligand interactions in the studied complexes are investigated by means of charge decomposition analysis, energy partitioning analysis (EPA), and natural bond orbital analysis. According to the EPA calculations, the electrostatic attraction is the dominant contribution to the M−S_2(R_2dtc) (dtc = dithiocarbamate) bonding. The electrostatic and the orbital energies follow the order of the total binding energy, and hence both contributions are responsible for the binding energy order of M(R_2dtc)$_2$ complexes. The stability of the M(R_2dtc)$_2$ complexes is estimated by means of calculated formation reaction energies in the gas phase and solution, and it decreases in the order Ni(R_2dtc)$_2$ > Cu(R_2dtc)$_2$ > Zn(R_2dtc)$_2$. Larger formation reaction energies are found for M(Et_2dtc)$_2$ than for M(Me_2dtc)$_2$ complexes. The calculations predict stabilization of M(II)(R_2dtc)$_2$ complexes going from the gas phase to a polar solvent and destabilization of the bidentate AgR_2dtc complex in a polar solvent. Gas-phase frequency calculations of all possible bonding types, symmetrical, asymmetrical, and uni- and bidentate, predict one band due to the ν(CS) IR absorption, and therefore the number of the bands in the 1060−920 cm^{-1} region could not be used to discern the metal−ligand bonding type. Periodic DFT frequency calculations for Cu(Et_2dtc)$_2$ reveal that the splitting observed in the solid-state spectra of the complexes arises from the nonplanar MS_4 fragment and intermolecular contacts but not from asymmetrical bonding. The calculations suggest that the important vibrational characteristic that can be used to discern uni- and bidentate bonding is the Raman activity of the ν(CS) band: It is very high for the unidentate dtc bonding (ν(C=S)) and low for the bidentate bonding (ν_{as}(CS)).

1. Introduction

Dithiocarbamates (dtc's) are a class of compounds with important chemical and biological properties. The high coordination ability of dtc to transition metals prompted intensive experimental and theoretical investigations of the metal dithiocarbamates.[1−6] Metal-chelating properties of dtc have attracted great attention because of their application in wide areas such as analytical methods for determination of heavy atoms,[7] industrial separation processes,[8] agriculture,[9] medicine,[10] and the rubber industry.[11] The biological activity of dtc is based on the complex formation of the active dtc group with metal atoms of metal-containing enzymes, producing enzyme inhibition.[12] The intensively utilized dtc fungicides influence the biological activity and physical properties of the soil as well as human health. It was established that dtc decomposition and elimination from the natural environment are slowed down because of dtc complexation with metals in soil. However, dithiocarbamate chelating agents have been used extensively to remove heavy metals from various wastewaters.[13−16] The effectiveness of the dtc reagents for heavy metal binding requires high selectivity and coordination ability of the ligands to the metal ions and stable precipitates that cannot decompose and release the metal to the environment during a short period of time. To obtain quantitative information on the thermodynamic stabilities of the metal dtc complexes, calorimetric measurements in solution, vacuum sublimation, and evaluation of stability constants have been carried out.[1,2] The global picture of the thermodynamic stability obtained from the experimental approaches consists of many coupled dissociation and association equilibria, and it does not give information on detailed structural possibilities and on their relative stabilities. Quantum chemical and spectroscopic studies could provide essential information on the structure, conformational behavior, and reactivity of dtc. The analysis of the theoretical results is important for understanding of the factors responsible for the coordination ability of dtc to different metal ions as well as for estimation of the mode and the strength of the M−S(dtc) bonding, the character of M−S interactions, and the stability of the metal complexes. Formation reaction energy calculations in the gas phase and solution give the possibility to evaluate the effect of the solvent. Deeper insight into the reactivity, stability, and M−dtc bonding would help the effective usage of chelating properties of dtc in diverse areas.

The first part of the present work describes the selection of an appropriate density functional theory (DFT) method by means of comparison with ab initio methods accounting for electron correlation (MP2 and CCSD methods) for the reference H_2dtc molecule and by comparison with X-ray structural data of Ni(Et_2dtc)$_2$, Cu(Et_2dtc)$_2$, and Zn(Et_2dtc)$_2$ (Et_2dtc = diethyldithiocarbamate). In the second part, we applied the method selected to obtain information about the geometries and stabilities of Ag(I), Ni(II), Cu(II), and Zn(II) complexes with R_2dtc ligands

---

* Author to whom correspondence should be addressed. E-mail: ivelina@svr.igic.bas.bg.

10.1021/jp075008a CCC: $37.00

(R= Me (methyl) or Et (ethyl)). The solvation effect has been computed using the polarized continuum model (PCM) based on a self-consistent reaction field.[17−19] A variety of structural arrangements such as uni- or bidentate with respect to the bonding of the thio group or cis/trans with respect to the relative position of the two dtc molecules are considered. The M−R_2dtc bonding mode and strength are evaluated on the basis of the binding energy calculations. The M−R_2dtc bonding character is estimated by means of energy partitioning analysis (EPA) of electrostatic, orbital, and repulsive energy contributions as well as by analysis of σ-donation and π-back-donation contributions to the donor−acceptor interaction. A theoretical vibrational study of different model metal complexes of R_2dtc is performed to find out vibrational criteria capable of discerning uni- or bidentate symmetrical and bidentate asymmetrical bonding types in the M−R_2dtc complexes. The effect of the molecular symmetry, the coupling of the ligand modes, and the effect of the N-substituent on the vibrational behavior of Ag(I)(R_2dtc) and M(II)$(R_2\text{dtc})_2$ are investigated and discussed. The solid-state effect on the vibrational pattern of the complexes is estimated by means of comparison of the results from the gas-phase calculations of Cu$(Et_2\text{dtc})_2$ with that from solid-state calculations.

2. Computational Details

Geometry optimization, harmonic vibrational, and conformational analyses are performed for H_2dtc, Me_2dtc, Et_2dtc, and their deprotonated forms. For selection of suitable DFT levels of calculations, the simplest H_2dtc and $H_2\text{dtc}^-$ molecules served as benchmark examples. Calculations with the nonhybrid BLYP functional[20,21] and the hybrid B3LYP[20,22] and BHLYP[20,23] functionals are done, and their reliabilities are checked using reference MP2 calculations (frozen inner shells)[24] and coupled-cluster CCSD calculations with singles and doubles substitutions (frozen core approximation and full electron correlation).[25] Previous theoretical studies have shown that the B3LYP functional is suitable also for geometry optimization of transition metal complexes.[26] For Ni(II), Cu(II), and Zn(II), the 6-311+G(d) basis set is used, for Ag(I) LANL2DZ, and for C, S, N, and H atoms the 6-31++G(d,p) basis set. For the M(II)−dtc complexes, the combined basis set will be referred as B1, and for Ag(I)−dtc as B2. B3LYP functional calculations are performed using the Gaussian 03 program package.[27] Atomic charges are obtained using the natural population analysis of Weinhold and Hirshfeld.[28] Basis set superposition error (BSSE) corrections to the M−R_2dtc binding energy were calculated for the B1 (B2) basis set using the counterpoise method.[29] The bonding situation in the M−R_2dtc complexes is investigated by means of energy partitioning analysis (EPA) and charge decomposition analysis (CDA). The EPA is based on the methods of Morokuma[30] and Ziegler and Rauk[31] as implemented in the ADF(2005.01) program package.[32] The partitioning scheme is performed at the PW91/TZP level[33] with B3LYP/B1(B2) optimized structures. In these calculations, the relativistic effects have been considered by means of the zero-order regular approximation (ZORA).[34,35] Within this method, the total bonding energy between two fragments, ΔE_b, is split into the three components

$$\Delta E_b = \Delta E_{\text{elstat}} + \Delta E_{\text{Pauli}} + \Delta E_{\text{orb}} \qquad (1)$$

ΔE_{elstat} (electrostatic interaction energy) is computed using the frozen electron density distribution of the fragments in the geometry of the complex. ΔE_{Pauli} represents the repulsive electron interactions between occupied orbitals, and ΔE_{orb} is the stabilizing orbital interaction due to the relaxation of the Kohn−Sham orbitals in the self-consistent field procedure. The bonding situation in the transition metal complexes of R_2dtc is investigated also in the frame of donor−acceptor interaction by means of CDA.[36] The CDA decomposes the Kohn−Sham determinant of a complex [ML] in terms of fragment orbitals of the chosen ligand L and the metal [M]. The [M] ← L donation, q[d], is then given by mixing of the occupied orbitals of L and vacant orbitals of [M]. The [M] → L back-donation, q[b], in return is given by the mixing of the occupied orbitals of [M] and vacant orbitals of L. The mixing of the occupied orbitals of both fragments gives the repulsive polarization term q, and the mixing of the unoccupied orbitals gives the residual term q[s]. The CDA calculations of the M$(R_2\text{dtc})_2$ complexes are performed with the 6-31G(d,p) basis set on all of the atoms (except for Ag(I)) because the larger B1 basis set including diffuse functions gave great negative values for the residual term. A similar deterioration of the CDA results by applying a larger basis set was reported already in the literature.[37]

The solvent effect of dimethylsulfoxide (DMSO) on the reaction formation energy for the M$(R_2\text{dtc})_2$ complexes is computed using a PCM.[17−19]

The periodic DFT calculations of Cu$(Et_2\text{dtc})_2$ are performed using the Vienna ab initio simulation package (VASP).[38] The DFT is parametrized in the local density approximation with the exchange−correlation functional proposed by Perdew and Zunger and corrected for nonlocality in the generalized gradient approximations using the Perdew−Wang91 (PW91) functional. The interaction between the core and the electrons is described using the projector augmented wave potentials for all atoms.

3. Results and Discussion

3.1. Molecular Geometries. *3.1.1. Geometry Calculations of R_2dtc (R = H, Me, or Et).* Conformational analysis of the neutral and deprotonated forms of alkyl dithiocarbamate (R_2-dtc) (R = H, Me, or Et) is performed in the gas phase (Figure 1). Several functionals, nonhybrid BLYP and hybrid B3LYP and BHLYP, with the 6-31++G(d,p) basis set are applied for the simplest H_2dtc and $H_2\text{dtc}^-$ species, and the results are referred to MP2 and CCSD calculations (Table 1). The BLYP, B3LYP, and BHLYP calculations predict the minimum structure of H_2dtc in C_s symmetry, whereas according to the MP2 and CCSD calculations the H_2dtc minimum is in C_1 symmetry. The C_1 symmetry lowers the energy by 0.1−0.17 kcal/mol than that of the C_s geometry and shows slightly out-of-plane deviation of the H atoms. The CCSD calculations with B3LYP and MP2 optimized structures reveal a small energy difference (0.03 kcal/mol), indicating the small effect of the calculated geometry. All DFT, MP2, and CCSD calculations predict a minimum in C_1 symmetry for the deprotonated $H_2\text{dtc}^-$ and out-of-plane deviation of the two S atoms. The energy difference between C_1 and C_s geometries at different levels varies between 0.01 and 0.7 kcal/mol. As compared to the CCSD bond lengths, the B3LYP calculated C−N bond length is in good agreement, whereas the C−S and S−H bond lengths are longer (with ∼0.01 Å). At the same time, BHLYP well reproduces the C−S and S−H bond lengths and gives shorter C−N distances (∼0.01−0.03 Å). BLYP calculations give the worst geometry parameters in comparison to the CCSD results. As compared to CCSD-(full) calculations, for H_2dtc the absolute deviation of the BHLYP bond lengths is 0.006 Å and of the B3LYP bond lengths is 0.008 Å, and for $H_2\text{dtc}^-$ it is 0.010 and 0.007 Å, respectively. Obviously, both DFT levels are appropriate for dtc geometry

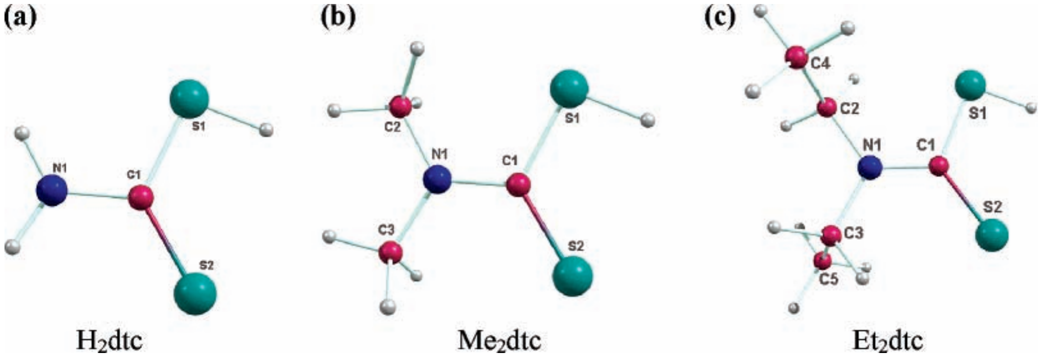

Figure 1. Optimized geometrires of (a) H_2dtc, (b) Me_2dtc, and (c) *trans*-Et_2dtc ligands at the B3LYP/6-31++G(d,p) level of theory.

TABLE 1: Calculated Geometrical Parameters of H_2dtc and H_2dtc^- Species at Different Levels of Theory with the 6-31++G(d,p) Basis Set

geometric parameters H_2dtc(CNS_2H_3)	BLYP C_s	B3LYP C_s	BHLYP C_s	CCSD[a]/full[b] C_s (imaginary frequencies)	MP2 C_s (imaginary frequencies)
C1−S2	1.678	1.658	1.647	1.651/1.649	1.641
C1−S1	1.820	1.795	1.772	1.782/1.779	1.779
S1−H	1.355	1.343	1.331	1.331/1.330	1.329
C1−N1	1.366	1.352	1.338	1.353/1.352	1.357
N1−H	1.018	1.010	1.001	1.006/1.006	1.008
	1.019	1.010	1.001	1.006/1.006	1.008
S1−C1−S2	125.2	124.7	124.4	124.8/124.7	125.0
S2−C1−N1	123.7	123.9	123.7	123.6/123.6	123.8

geometric parameters H_2dtc^-($CNS_2H_2^-$)	BLYP C_1	B3LYP C_1	BHLYP C_1	CCSD[a]/full[b] C_1	MP2 C_1
C1−S2	1.733	1.718	1.706	1.707	1.697
C1−S1	1.733	1.718	1.706	1.707	1.697
C1−N1	1.402	1.383	1.359	1.390	1.398
N1−H	1.02	1.011	0.999	1.008	1.010
	1.020	1.011	0.999	1.008	1.010
S1−C1−S2	128.2	127.9	127.6	127.8	128.0
S2−C1−N1	115.9	116.0	116.2	116.1	116.0

[a] Valence electrons are included in a correlation calculation. [b] All electrons are included in a correlation calculation.

SCHEME 1: Resonant Structures of R_2dtc− Species

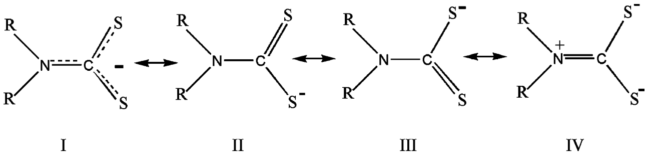

calculations. We selected the B3LYP functional for all calculations because the B3LYP geometry for the active ligand form, H_2dtc^-, in the metal complexation reaction is in best agreement with the CCSD results. Further, the ligand calculations are performed at the B3LYP/6-31++G(d,p) level. The neutral Me_2dtc and the deprotonated Me_2dtc^- species are minima in C_1 symmetry. Generally, the C, N, and S atoms are obtained approximately in a plane, and the CH_3 groups are asymmetric (Figure 1b). According to the calculations, the neutral and the deprotonated Et_2dtc species have two minima with cis and trans orientations of the ethyl radicals. The trans conformation of the neutral form is more stable by 0.7 kcal/mol, and that of the deprotonated form by 5.1 kcal/mol (Figure 1c).

Different resonant structures are possible for H_2dtc^-, Me_2dtc^-, and Et_2dtc^-, as shown in Scheme 1. Natural bond orbital (NBO) analysis of the deprotonated ligands, H_2dtc^-, Me_2dtc^-, and Et_2dtc^-, could suggest the most probable resonant structure, and the data obtained are given in Table 2. As seen in Table 2, the shortest C1−N1 bond length and double bond character of the bond for H_2dtc^- reveal the resonant structure IV, whereas double bond character of the C−S bond for Me_2dtc^- and Et_2dtc^- indicates resonant structures II and III, respectively. On the basis of the occupation percentage obtained from the NBO analysis, C1 → N1 and S1(2) → C1 σ bond polarizations are predicted. That is important information used below to explain the bond length changes upon the metal interaction.

TABLE 2: Selected Calculated Bond Lengths (in Å) of R_2dtc (R = H, Me, or Et) and R_2dtc^- and Natural Bond Orbital Analysis of Deprotonated Species at the B3LYP/6-31++G(d,p) Level

bond[a]	H_2dtc	Me_2dtc	*trans*-Et_2dtc	H_2dtc^-	Me_2dtc^-	*trans*-Et_2dtc^-
S1−H	1.343	1.344	1.344			
C1−S1	1.795	1.805	1.809	1.718	1.728	1.728
pol				58:42(σ)	58:42(σ) 25:75(π)	58:42(σ)
C1−S2	1.658	1.671	1.675	1.718	1.728	1.728
pol				58:42(σ)	58:42(σ)	58:42(σ) 25:75(π)
C1−N1	1.352	1.352	1.351	1.383	1.393	1.389
pol				38:62(σ) 18:82(π)	36:64(σ)	36:64(σ)
N1−C2		1.466	1.473		1.452	1.463
N1−C3		1.467	1.476		1.452	1.463

[a] Atom numbering is given in Figure 1. Pol is the percentage of occupancy assigned to the first and second atoms.

3.1.2. Geometry Calculations for M(Et_2dtc)$_2$ (M═Ni(II), Cu(II), or Zn(II)). Table 3 gives selected calculated and experi-

TABLE 3: Calculated Geometrical Parameters of $M(Et_2dtc)_2$ (M = Ni(II), Cu(II), or Zn(II)), Compared to the Experimental Values (Bond Lengths, *R*, in Å; Bending Angles, *A*, in deg)

	$Ni(Et_2dtc)_2$ (LS)		$Cu(Et_2dtc)_2$			$Zn(Et_2dtc)_2$	
geometry	expt[a]	B3LYP/B1	expt[b]	B3LYP/B1	PW91[c]	expt[d]	B3LYP/B1
R(M−S1)	2.207(2)	2.253 (2.375 HS)	2.317(2)	2.359	2.325	2.443(3)	2.391
R(M−S2)	2.195(2)	2.253 (2.375 HS)	2.297(2)	2.359	2.324	2.355(3)	2.392
R(M−S1′)		2.253 (2.375 HS)	2.301(2)	2.359	2.322	2.331(3)	2.393
R(M−S2′)		2.253 (2.375 HS)	2.339(2)	2.359	2.330	2.815(2)	2.391
R(S1−C1)	1.700(7)	1.731	1.711(8)	1.735	1.723	1.722(10)	1.745
R(S2−C1)	1.713(7)	1.731	1.713(8)	1.735	1.721	1.725(10)	1.744
R(C1−N1)	1.33(10)	1.338	1.350(10)	1.340	1.344	1.340(13)	1.342
R(N1−C2)	1.49(13)	1.473	1.470(12)	1.475	1.468	1.440(14)	1.476
R(N1−C3)	1.48(17)	1.473	1.470(11)	1.475	1.471	1.490(15)	1.476
R(C2−C4)	1.50(15)	1.531	1.520(16)	1.532	1.527	1.520(18)	1.531
R(C3−C5)	1.53(22)	1.531	1.520(17)	1.532	1.527	1.480(22)	1.531
R(S1′−C1′)		1.731	1.708(7)	1.735	1.721	1.723(10)	1.744
R(S2′−C1′)		1.731	1.736(7)	1.735	1.722	1.737(9)	1.745
R(C1′−N1′)		1.338	1.330(8)	1.340	1.344	1.310(12)	1.342
R(N1′−C2′)		1.473	1.46(1)	1.475	1.469	1.480(15)	1.476
R(N1′−C3′)		1.473	1.48(1)	1.475	1.467	1.480(14)	1.476
R(C2′−C4′)		1.531	1.530(15)	1.532	1.527	1.510(21)	1.531
R(C3′−C5′)		1.531	1.510(17)	1.532	1.527	1.530(20)	1.531
A(S1−M−S2)	79.11(11)	78.77	77.19 (9′)	76.40	76.68	75.47′(13)	77.19
A(S1′−M−S2′)		78.77	76.27 (9′)	76.40	76.68	69.34′(12)	77.18
A(M−S1−C1)	85.25(26) 84.44(26)	84.94	83.43 (28′)	84.60	84.68	81.53′(35)	82.61
A(S1−C1−S2)	110.34(37)	111.35	114.36 (40′)	114.4	113.72	117.32′(51)	117.55
A(S1′−C6−S2′)		111.35	112.56 (35′)	114.4	113.86	117.47′(49)	117.55

[a] See ref 39. [b] See ref 40. [c] Calculations with VASP. [d] See ref 41.

mental bond lengths and bond angles of $Ni(Et_2dtc)_2$, $Cu(Et_2dtc)_2$, and $Zn(Et_2dtc)_2$ complexes. The optimized compounds are presented in Figure 2. Experimental structural data for the compounds are available from X-ray diffraction analysis.[39−41] The calculations of high-spin (HS, ^{3}Bu) and low-spin (LS, ^{1}Ag) states of $Ni(Et_2dtc)_2$ in C_{2h} symmetry revealed stabilization of the low-spin state by 1.4 kcal/mol. According to the calculations, the M−S bond lengths for $M(Et_2dtc)_2$ increase in the order Ni−S (LS) < Cu−S < Zn−S, and this trend is consistent with the experimental one. Similar M−S bond lengths and the same order are calculated for $M(Me_2dtc)_2$ complexes. In the case of high-spin $Ni(Et_2dtc)_2$ calculations, other orders of M−S bond lengths are obtained: Cu−S < Ni−S (HS) < Zn−S. Therefore, it could be expected that the DFT/B3LYP/B1 level will correctly predict the spin state of the transition metal complexes of R_2dtc. In line with the experiment, $Ni(Et_2dtc)_2$ and $Cu(Et_2dtc)_2$ structures are minima in C_{2h} symmetry (Figure 2a). The geometry optimization of the $Zn(Et_2dtc)_2$ complex in C_{2h} symmetry showed one imaginery frequency (-40 cm^{-1}). The C_1 structure is more stable by 8.1.kcal/mol. The relaxed structure of $Zn(Et_2dtc)_2$ has a bite angle of A(S1−Zn−S2′) = 128° and obviously leans toward tetrahedral symmetry; however, the ultimate boundary case (where A(S1−Zn−S4) = 109°) has not been reached (Figure 2b). The calculated minima of $M(Et_2dtc)_2$ complexes show trans positions of the ethyl substituents of one dtc ligand in agreement with their X-ray structures. The stabilization of two *trans*-Et_2dtc ligands in the metal complexes could be explained with a more stable *trans*-Et_2dtc conformation (Figure 1c) than the cis one. The average deviations of the bond lengths from the corresponding experimental values are 0.024 Å for $Ni(Et_2dtc)_2$, 0.019 Å for $Cu(Et_2dtc)_2$, and 0.046 Å for $Zn(Et_2dtc)_2$. The B3LYP/B1 M−S bond lengths are longer (by 0.04−0.09 Å) than the experimental ones (considering the average experimental M−S bond length). $Zn(Et_2dtc)_2$ shows the largest deviation of the calculated geometry data from the experimental data. This difference is due to the intermolecular interactions in the solid state, producing dimer formation. (The metal atom is five-coordinate.[41]) Detailed vibrational investigations on $Zn(Et_2dtc)_2$ in the solid state and in solution predicted higher molecular symmetry in solution due to the removal of the intermolecular interaction in the crystal. Thus, in solution zinc is four-coordinate, and the ZnS_4 chromophore polyhedron approaches T_d geometry.[42] Because of the lack of the fifth Zn−S contact, the $Zn(Et_2dtc)_2$ geometry in solution is expected to be close to that in the gas phase. The calculations of isolated $M(Et_2dtc)_2$ molecules indicate that all four M−S bond lengths are equalized. Obviously, the observed asymmetrical bidentate M−S bonding is produced mainly from the crystal packing effect (Table 3). The molecular geometry of $Cu(Et_2dtc)_2$ obtained from the solid-state calculations is in better agreement with the X-ray data. The calculations are performed for the monoclinic unit cell of $Cu(Et_2dtc)_2$ with the dimensions $a = 9.907$, $b = 10.627$, and $c = 16.591$ Å taken from X-ray diffraction analysis.[40] In contrast to the calculated gas-phase geometry of $Cu(Et_2dtc)_2$, the periodic DFT calculations, simulating the solid state, predicted different M−S bond lengths, i.e., asymmetrical bonding. On the basis of the reference CCSD calculations and available experimental geometries, the DFT/B3LYP/B1 method is selected as the appropriate one for the theoretical consideration of R_2dtc (R = H, Me, or Et) and their metal complexes.

3.2. Analysis of the M−R_2dtc Bonding Situation. *3.2.1. Binding Energies.* The M−dtc bonding situation and the electron density distribution for AgR_2dtc and $M(II)(R_2dtc)_2$ (M(II) = Ni(II), Cu(II), or Zn(II); R = Me or Et) were investigated in terms of NBO analysis, EPA, and CDA. The M−S(dtc) binding energy and the most important data for the bonding analysis for the interactions between one R_2dtc ligand and one MR_2dtc

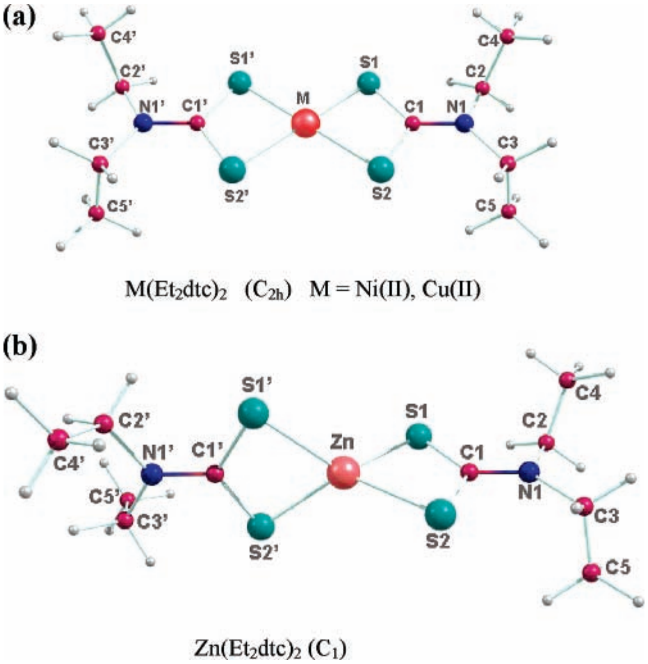

Figure 2. Optimized geometries of (a) Ni(Et$_2$dtc)$_2$ and Cu(Et$_2$dtc)$_2$ and (b) Zn(Et$_2$dtc)$_2$ complexes at the B3LYP/B1 level of theory.

TABLE 4: Binding Energy M−S$_2$ (R$_2$dtc) (ΔE_b) and Energy Partitioning Analysis of M−R$_2$dtc Complexes (Bond Length, R, in Å, Energies in kcal/mol)

			EPA (PW91/TZP)			
compound	R(M−S)	ΔE_b[a] (B3LYP/B1(B2)[b])	ΔE_b[a]	ΔE_{elstat}	ΔE_{orb}	ΔE_{Pauli}
Ni(Me$_2$dtc)$_2$	2.252	−190.5 (106.1)[c]	−200.7	−199.1	−118.5	116.9
Cu(Me$_2$dtc)$_2$	2.359	−170.8 (87.2)[c]	−178.1	−184.9	−93.9	100.6
Zn(Me$_2$dtc)$_2$	2.395	−182.5	−188.0	−187.6	−102.1	101.8
bi-AgMe$_2$dtc	2.594	−171.6	−186.1	−196.4	−65.4	75.7
uni-AgMe$_2$dtc	2.431	−158.4				
Ni(Et$_2$dtc)$_2$	2.253	−188.6 (108.5)[c]	−198.3	−196.9	−118.7	117.3
Cu(Et$_2$dtc)$_2$	2.359	−168.2 (89.4)[c]	−175.7	−182.9	−94.4	101.6
Zn(Et$_2$dtc)$_2$	2.392	−180.5	−185.2	−184.6	−103.3	102.8
bi-AgEt$_2$dtc	2.586	−171.3	−185.4	−195.7	−66.7	76.9
uni-AgEt$_2$dtc	2.429	−157.6				

[a] $\Delta E_b = E(M(R_2dtc)_2) - E(MR_2dtc^+) - E(R_2dtc^-)$ for M = Ni(II), Cu(II), or Zn(II), and $\Delta E_b = E(AgR_2dtc) - E(Ag^+) - E(R_2dtc^-)$. [b] The B1 basis set is for M(II)(R$_2$dtc)$_2$ complexes, and the B2 basis set is for AgR$_2$dtc complexes; see Computational Details section. ΔE_b at the B3LYP/B1(B2) level are BSSE corrected values. [c] Available experimental data for ΔE_b are given in brackets; see ref 3 for Ni(Me$_2$dtc)$_2$ and Cu(Me$_2$dtc)$_2$, ref 44 for Ni(Et$_2$dtc)$_2$, and ref 45 for Cu(Et$_2$dtc)$_2$.

(or Ag) fragment are given in Table 4. The binding energy obtained from the Gaussian program is calculated with frozen fragment geometries at the complex geometry. Natural atomic charges of metal ions and CDA data, calculated for a series of complexes, Ni(R$_2$dtc)$_2$, Cu(R$_2$dtc)$_2$, Zn(R$_2$dtc)$_2$, and AgR$_2$dtc, are given in Table 5. The bidentate M(Me$_2$dtc)$_2$ structures are minima in C_1 symmetry. (The minima of M(Et$_2$dtc)$_2$ structures were discussed in the previous section.) The unidentate AgR$_2$dtc complexes are minima in C_1 symmetry, the bidentate AgMe$_2$dtc is a minimum in C_{2v} symmetry, and the bidentate AgEt$_2$dtc is a minimum in C_2 symmetry. The bidentate AgR$_2$dtc complexes are more stable by ∼17 kcal/mol than the unidentate ones.

The metal−ligand bonding in R$_2$dtc complexes is described using the charged fragments M(R$_2$dtc)$^+$ + R$_2$dtc$^-$ for M = Ni^{2+}, Cu^{2+}, or Zn^{2+} and M$^+$+ R$_2$dtc$^-$ for M = Ag$^+$ as bonding partners. The bonding situation could be analyzed also using the neutral fragments M(R$_2$dtc)$^•$ + R$_2$dtc$^•$, and the values of the fragment charges should suggest which bonding situation better describes the M−L bonding in the M(R$_2$dtc)$_2$ complexes. The Hirshfeld approach gives positive charges of M(R$_2$dtc)$^+$, 0.46e for Ni(R$_2$dtc)$^+$, 0.44e for Cu(R$_2$dtc)$^+$, and 0.51e for Zn(R$_2$dtc)$^+$, and negative charges for R$_2$dtc (−0.43e to −0.51e). Thus, the M(R$_2$dtc)$_2$ complexes appear to be a borderline case of the two bonding situations. It should be mentioned that the Hirshfeld charges are chemically meaningful whereas the NBO model predicts often too large ionic character.[43] To describe the bonding situation in the metal complexes of R$_2$dtc, we select the ionic fragments. However, in this case an overestimation of the electrostatic contribution is expected, and it should be taken into account.

TABLE 5: Atomic Charges (q) of Ni(II), Cu(II), Zn(II) and Ag(I) in the M−R$_2$dtc Complexes Using Natural Population Analysis (at the B3LYP/B1 Level), Hirshfeld Analysis (at the PW91/TZP Level) and Charge Decomposition Analysis (at the B3LYP/6-31G(d,p) Level)[a]

	charge		CDA			
system	q(M) NPA	q(M) Hirshfeld	q[d]	q[b]	q[r]	q[s]
Ni(Me$_2$dtc)$_2$	0.524	0.430	0.713	0.046	−0.233	−0.105
Cu(Me$_2$dtc)$_2$	0.867	0.491	0.626	0.044	−0.054	−0.089
Zn(Me$_2$dtc)$_2$	1.298	0.612	0.801	0.034	−0.088	−0.083
uni-AgMe$_2$dtc	0.474		0.583	0.034	−0.067	−0.070
bi-AgMe$_2$dtc	0.674		0.867	0.029	−0.131	−0.066
Ni(Et$_2$dtc)$_2$	0.525	0.421	0.714	0.046	−0.238	−0.105
Cu(Et$_2$dtc)$_2$	0.867	0.480	0.650	0.045	−0.074	−0.090
Zn(Et$_2$dtc)$_2$	1.303	0.600	0.797	0.035	−0.087	−0.085
uni-AgEt$_2$dtc	0.482		0.625	0.040	−0.075	−0.073
bi-AgEt$_2$dtc	0.676		0.870	0.030	−0.133	−0.065

[a] q[d], donation L → M(II); q[b] back-donation M(II) → L; q[r], repulsive polarization; q[s] nonclassical rest term.

First, the binding energies (ΔE_b) of M^{2+} with one R$_2$dtc$^-$ ligand are calculated. ΔE_b (absolute value) decreases in the order Ni(R$_2$dtc)$^+$ > Cu(R$_2$dtc)$^+$ > Zn(R$_2$dtc)$^+$ in agreement with the increasing M−S bond length order. The evaluation of the M−L binding energy in the complexes with two R$_2$dtc$^-$, however, is more complicated. The M−L binding energy (absolute value) calculated on the basis of the charged fragments decreases in the order Ni−S$_2$ (Ni(R$_2$dtc)$_2$) > Zn−S$_2$ (Zn(R$_2$dtc)$_2$) > Ag−S$_2$ (AgR$_2$dtc) > Cu−S$_2$ (Cu(R$_2$dtc)$_2$) (Table 4). The average metal−sulfur bond-dissociation enthalpies $\langle D_m \rangle$(M−S) in M(Me$_2$dtc)$_2$ have been experimentally derived, and the larger D_m(Ni−S) value as compared to the D_m(Cu−S) value correlates with the calculated ΔE_b trend: Ni−S(R$_2$dtc) > Cu−S(R$_2$dtc).[3,44,45] The M−S binding energy slightly depends on the Me/Et-substituent (∼2 kcal/mol), and larger M−S bond strength is found for R = Me as compared to R = Et$_2$dtc. Although the binding energies from EPA (ADF) and the dissociation energies obtained from the Gaussian program are not equivalent, both approaches give the same trend of binding energies for M(R$_2$dtc)$_2$ complexes (Table 4). According to the calculations, the electrostatic attraction between the charged fragments in all complexes studied has a predominant contribution to the M−S$_2$(R$_2$dtc) bonding. Very important information about the covalent bonding situation comes from the orbital term ΔE_{orb}. The orders of the electrostatic attractions and the orbital interactions follow the trend of the total binding energy, and obviously both contributions are responsible for the binding energy order. A survey of the metal atomic charges of M(R$_2$dtc)$_2$ reveals that they increase in the order Ni(II) < Cu(II) <

Zn(II). Lower metal atomic charge indicates larger M → L charge transfer and hence more covalent bond. Our results show that the order of the evaluated M → L charge transfer in Cu-$(R_2dtc)_2$ and Zn$(R_2dtc)_2$ does not correlate with the order of the orbital interaction. As discussed in the literature, the information obtained from the atomic charges must be used with caution, and a partitioning of the interaction energy is advisable when the chemical bond is analyzed in terms of covalent and electrostatic contributions.[46]

The calculated values of the Pauli repulsion energy give information about the metal−ligand interactions. The Pauli repulsion between the charged fragments in M$(R_2dtc)_2$ is the largest one for the Ni(II) complexes and decreases in Zn(II) and Cu(II) complexes.

A strong Ag−S bonding (comparable with Zn−S(R_2dtc)) is found for the bidentate AgR_2dtc complexes, which arises mainly from the large electrostatic attraction contribution. Among the complexes studied, AgR_2dtc shows the weakest orbital interaction and Pauli repulsion interaction.

To estimate the σ-donation (metal ← ligand) and the π-back-donation (metal → ligand) contributions, the M−S_2(R_2dtc) bonding is studied in terms of donor−acceptor interaction between the closed-shell ligand and the closed-shell metal fragments using the CDA partitioning scheme.[36] The CDA data are given in Table 5. Among the bis-M$(R_2dtc)_2$ complexes, the largest donation is calculated for the Zn(II) complex, followed by the Ni(II) and Cu(II) complexes. The L → M donation trend could be understood by examining the radii of the valence s- and d-orbitals. The electronic ground states of Ni(II), Cu(II), and Zn(II) ions are d^8s^0, d^9s^0, and $d^{10}s^0$, their valence s-orbitals serve as acceptor orbitals, and the valence d-orbitals are the donor orbitals. The radius of the valence s-orbitals increases in the order Zn(1.200 Å) < Ni(1.276 Å) < Cu(1.374 Å), which is in agreement with the decreasing donation in the same order. As the π-back-donation strongly depends on the bond length, the π-back-donation interaction increases with decrease of the bond distances in the order Zn−S > Cu−S > Ni−S. However, the back-donation contributions were found to be very small, and the donation contributions appeared dominant.

The repulsion interaction estimated by CDA is in agreement with the calculated Pauli repulsion above. The negative values for the repulsive polarization q indicate the depleted charge from the overlapping area of the occupied orbitals. The largest value of the occupied/occupied repulsion term for Ni−R_2dtc bonding reveals a significant charge organization. The calculations suggest that for the Ni(II) complex the d_{xy} orbital is unoccupied and for the Cu(II) complex the d_{xy} orbital contains an unpaired d-electron. The minimal occupation of the d_{xy} orbital along M−S bonding decreases the d_σ−s_σ repulsion during the M−R_2dtc interaction.

The orbital energies of Ni(II), Cu(II), and Zn(II) shown in Figure 3 are also important for a complete understanding of the M(II)−R_2dtc bonds. The interaction of the filled S(dtc) σ-donor orbital with the filled (d_σ) metal atomic orbital leads to σ-repulsion. In general, sd_σ mixing in the metal center shifts the electron density away from the M−S bond to the xy plane, decreasing the σ-repulsion and allowing for a shorter bond. The degree of the s−d_σ mixing depends on the s−d_σ gap. The Ni(II) ion, with the smallest s−d_σ energy gap, forms the shortest Ni−S bond lengths, whereas the Zn(II) ion with the largest s−d_σ energy gap gives the longest Zn−S bond lengths (Table 3).

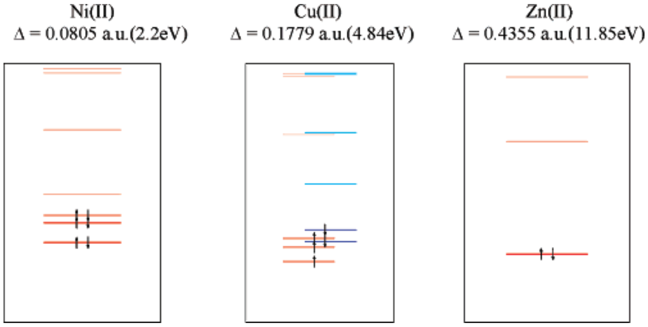

Figure 3. Orbital energy diagram for the highest occupied (d) and lowest unoccupied (s) atomic orbitals for Ni^{2+}, Cu^{2+}, and Zn^{2+}.

TABLE 6: Calculated Formation Reaction Energies (ΔE_r) and Gibbs Free Reaction Energies (ΔG_r) for the Gas Phase and Solution of M−R_2dtc Complexes (Energies in kcal/mol)

compound	$-\Delta E_r^{gs}$	$-\Delta E_r^{sol}$	$-\Delta G_r^{sol}$
Ni$(Me_2dtc)_2$	37.3	60.0/53.8[a]	71.4
Cu$(Me_2dtc)_2$	36.7	57.2/50.9[a]	69.1
Zn$(Me_2dtc)_2$	32.9	46.5/43.7[a]	64.1
bi-AgMe_2dtc	19.5	12.7[a]	
uni-AgMe_2dtc	3.1	6.9[a]	
Ni$(Et_2dtc)_2$	38.1	60.3[a]	
Cu$(Et_2dtc)_2$	38.0	57.4[a]	
Zn$(Et_2dtc)_2$	34.1	50.3[a]	
bi-AgEt_2dtc	19.8	15.6[a]	
uni-AgEt_2dtc	2.1	7.9[a]	

[a] Continuum solvation calculations without geometry optimization.

3.3. Formation Energies. The metal complexes of R_2dtc reveal their interesting chemical behavior in solution, and therefore we extended our theoretical studies to include calculations of solvated systems. The formation reaction energies (ΔE_r) of M$(R_2dtc)_2$ (M = Ni(II), Cu(II), or Zn(II)) as well as of uni- and bidentate AgR_2dtc (R = Me or Et) complexes are calculated in the gas phase and solution. The solvent effects are estimated using a polar solvent (DMSO). In the case of a small specific interaction of the solvent (microsolvation), the continuum solvation results obtained for DMSO should be valid for other polar solvents as well. From the other side, it is expected that the energetic results valid for a nonpolar solvent are similar to those in the gas phase because the geometry in a nonpolar solution is slightly affected and the solvation contribution is insignificant. The formation reaction energies of M−R_2dtc complexes in the gas phase and solution are calculated according to the following reaction scheme

$$M(NO_3)_2(g/s) + 2NaR_2dtc(g/s) \rightarrow M(R_2dtc)_2(g/s) + 2NaNO_3(g/s) \quad (2)$$

$$AgNO_3(g/s) + NaR_2dtc(g/s) \rightarrow AgR_2dtc(g/s) + NaNO_3(g/s) \quad (3)$$

All species of the reactions with R = Me_2dtc are optimized in solution, and the calculations are performed with minima structures. It is found that continuum solvent interaction produces insignificant shortening of the M−S bond length, visible shortening of the C1−N1 bond length (∼0.012 Å), and elongation of the C1−S (0.010 Å) and N1−C2 (∼0.04 Å) bond lengths. For the gas phase and solution, the formation reaction energies, ΔE_r, given in Table 6, are negative, indicating that the complex formation process is thermodynamically favored. The formation reaction energies (absolute values) decrease in the order Ni$(Me_2dtc)_2$ > Cu$(Me_2dtc)_2$ > Zn$(Me_2dtc)_2$. The solvent effect lowers the ΔE_r value of the M$(R_2dtc)_2$ complexes by 13−23 kcal/mol. In addition to the ΔE_r value in solution, we computed the Gibbs reaction energies, ΔG_r (Table 6). The inclusion of the thermochemical corrections does not change the formation reaction energy order; it only leads to more negative energies by 11−17 kcal/mol. The calculated formation reaction energies are in agreement with the available experimental data for $Cu(Me_2dtc)_2$ and $Ni(Me_2dtc)_2$ complexes, revealing a more negative standard molar enthalpy of formation in solution for the Ni(II) complex (−34.9 kcal/mol) than that for the Cu(II) complex (−20.4 kcal/mol).[2] The order and the difference of the calculated ΔH_r values for Cu(II) and Ni(II) complexes follow the experiment, the calculated ΔH_r enthalpies being ~33 kcal/mol more negative. However, it is difficult to compare the results closely because we calculate specific substitution reactions while in the experimental analysis a global modeling of a complex set of reactions has been performed.

The solvation energies of Ag(I)R_2dtc and M(II)$(Et_2dtc)_2$ are calculated by means of single-point continuum solvation calculations because the geometry changes produced by the solvation of M(II)$(Me_2dtc)_2$ are found to be small (~0.2 kcal/mol). As seen from Table 6, the geometry changes in solution lead to an increase of the formation reaction energies (obtained from single-point continuum solvation calculations) of the M(II)$(Me_2dtc)_2$ complexes up to 6.3 kcal/mol, but the order of the calculated ΔE_r value in solution is the same. The ethyl substituent does not change the order of the formation reaction energies obtained for M(II)$(Me_2dtc)_2$. According to the ΔE_r calculations in the gas phase and solution, slightly larger stabilization is suggested of M(II)$(Et_2dtc)_2$ complexes than that of M(II)$(Me_2dtc)_2$, and this result correlates with experimental data showing that the metal−sulfur bond-dissociation enthalpies of $D_m(M-S)_{Et}$ are larger than that of $D_m(M-S)_{Me}$.[3] This finding, however, is not in line with the M−S bonding strengths. It should be remarked that the available experimental thermochemical data for $Ni(R_2dtc)_2$ and $Cu(R_2dtc)_2$ complexes can be interpreted in various ways depending on the purposes for which these data are required.[2,3] Metal−ligand binding energies can in principle be considered in the context of bond-energy schemes or in terms of bond-dissociation energies, and the applicabilities of these approaches are quite different. The bond-energy schemes are not easily applied to coordination compounds, whereas the dissociation energies are not a direct measure of the binding energies due to the reorganization energies of the radicals. For that reason, the explicit comparison of the calculated energetic and thermochemical data with the experiment is complicated and should be performed with caution.

The comparison between uni- and bidentate AgR_2dtc reaction formation energies in the gas phase and solution reveals that ΔE_r is larger for the bidentate species. It is interesting to note that the solvent effect produces a decrease of the reaction energy for the bidentate AgR_2dtc and an increase of the reaction energy for the unidentate AgR_2dtc. The calculations predict similar reaction energies for the bidentate AgMe_2dtc and AgEt_2dtc in the gas phase, and it is larger for AgEt_2dtc in solution.

As was found above, the calculated larger reaction energy (absolute value) of $Ni(R_2dtc)_2$ than that of $Cu(R_2dtc)_2$ is in agreement with the experimental formation enthalpies of the complexes. However, this finding does not correlate with the stability order of $Ni(Et_2dtc)_2$ < Cu((Et_2dtc)$_2$ established on the basis of metal exchange reactions between divalent metal ions and their dithiocarbamate complexes in DMSO.[1] Because the two experimental techniques provide different results for the $M(R_2dtc)_2$ stability order, it could be suggested that (1) the experiments need to be refined or (2) specific solvent interactions have a decisive effect on $M(R_2dtc)_2$ stability.

The calculated formation reaction energies in solution indicate that among the four metals in the environment Ni(II) is the metal that most likely should inhibit the transformation reaction of dtc in soil followed by Cu(II), Zn(II), and Ag(I).

3.4. Vibrational Study of the Bonding Type in M−R_2dtc Complexes (M = Ag(I), Ni(II), Cu(II), or Zn(II)). The precise characterization of the metal complexes of R_2dtc in the environment requires vibrational criteria, capable of discerning the bonding type in the M−dtc complexes when X-ray diffraction data are not available. Previously, the M−dtc bonding type was suggested using the popular Bonati−Ugo method, based on experimentally derived vibrational criteria.[47] However, detailed comparison of the X-ray diffraction data for M(II)$(R_2dtc)_2$ and M(III)$(R_2dtc)_2$ showed that the dtc ligands, irrespective of the host complex or the ligand bonding type, are at sites of C_1 symmetry, thus ruling out the possibility of detecting the ligand bonding type from the solid-state vibrational spectra.[48] The present vibrational study is based mainly on DFT calculations and aims first at reliable assignment of the vibrational molecular modes and second at a better understanding of the established correlation between the ν_{as}(CS) vibrational behavior and the metal−ligand bonding type. For that purpose, a number of M−R_2dtc model complexes are considered: M = Ag(I), Cu(II), Ni(II), or Zn(II); R = Me or Et. Uni- and bidentate bonding types of the dtc ligands are modeled: (i) for Ag(R_2dtc) in a ratio of M/R_2dtc = 1:1 and (ii) for $Cu(R_2dtc)_2$ in a ratio of M/R_2dtc = 1:2. Both symmetrical and asymmetrical bidentate bonding of the dtc ligand (with equivalent and nonequivalent M−S bond lengths) are simulated and studied with the help of model complexes. The effect of the molecular symmetry, the coupling of the ligand modes, and the effect of the N-substituents on selected characteristic vibrational modes are discussed. A new approach was applied to study the crystal packing effect on the complex vibrational pattern: Periodic DFT calculations (using the VASP program) are performed for $Cu(Et_2dtc)_2$, and the frequencies obtained are compared with the data calculated for the isolated complex.

3.4.1. Vibrational Analysis of $M(Et_2dtc)_2$ (M = Ni(II), Cu(II), or Zn(II)). First, frequency calculations are performed for complexes with known crystal and molecular structures ($Ni(Et_2dtc)_2$, $Cu(Et_2dtc)_2$, and $Zn(Et_2dtc)_2$) with the purpose of reliable interpretation of the observed vibrational spectra. The M(II)−Et_2dtc bonding type in these structures is symmetrical bidentate. The full list of calculated and experimental spectra of the $M(Et_2dtc)_2$ complexes is given in Table 1S of the Supporting Information. Selected calculated and experimental vibrational frequencies of $M(Et_2dtc)_2$ complexes discussed in detail as to the ligand bonding type are given in Table 7. In general, DFT/B3LYP/B1 calculated frequencies were found to be in reasonable agreement with the observed vibrational spectra of $M(Et_2dtc)_2$ complexes.

The frequency calculations for $Ni(Et_2dtc)_2$ and $Cu(Et_2dtc)_2$ structures are performed at the optimized geometry in C_{2h} symmetry (Table 7). Because the ν(CS) modes were considered as indicative for the metal−ligand bonding type, below we mainly discuss its vibrational behavior. Two bands due to the ν_{as}(CS) modes and two bands due to the ν_s(CS) modes should appear for $M(Et_2dtc)_2$ in the 1060−920 and ~900−800 cm^{-1} regions, respectively.[48] For C_{2h} symmetry, one of the ν_{as}(CS) vibrations is IR-active (B_u), and the other one is Raman-active (B_g). Hence, in the IR spectra of $Ni(Et_2dtc)_2$ and $Cu(Et_2dtc)_2$, only one ν_{as}(CS) band should appear. On the basis of the calculations, the intense IR bands observed at 993 cm^{-1} for $Ni(Et_2dtc)_2$ and at 996 cm^{-1} for $Cu(Et_2dtc)_2$ are assigned to the

TABLE 7: Calculated (Scaled, Scaling Factor = 0.985) Frequencies, IR Intensity (I_{IR}) and Raman Activity (A_{Ra}) of Ni(Et_2dtc)$_2$, Cu(Et_2dtc)$_2$, Zn(Etdtc)$_2$ at B3LYP/B1 Level and Comparison with Experimental IR Spectra

Ni(Et_2dtc)$_2$			Cu(Et_2dtc)$_2$						Zn(Et_2dtc)$_2$				
	calcd (C_{2h})			calcd (C_1)			calcd (C_{2h})		expt		calcd (C_1)		
expt	frequency	I_{IR}/A_{Ra}	expt	frequency[a]	frequency[b]	I_{IR}/A_{Ra}	frequency[c]	I_{IR}/A_{Ra}	solid	sol^{CH_2Cl_2}	frequency	I_{IR}/A_{Ra}	assignment
	1518(Ag)	0/65		1478	1515	39/56	1514 (Ag)	0/59			1515	0/59	$\delta(CH_3) + \nu(SC-N)$
1495vs	1514(Au)	677/0	1505s	1472	1511	588/2	1511 (Au)	616/0	1508vs	1500vs	1513	390/13	$\delta(CH_3) + \nu(SC-N)$
	1459(Ag)	0/40		1418	1455	65/33	1454 (Ag)	0/50			1450	5/7	$\nu(SC-N)^s + \delta(CCH)$
1435 m	1458(Au)	374/0	1435s	1418	1453	307/9	1454 (Au)	378/0	1435s	1437vs	1450	359/6	$\nu(SC-N)^{as} + \delta(CCH)$
993s	995(Bu)	40/0	996s	996	991	44/0	989 (Bu)	44/0	995s	989s	982	36/4	$\nu(CS)_{as}$
972sh	987(Bg)	0/20	974sh	974	982	0/37	981 (Bg)	0/41	983 sh		981	36/3	$\nu(CS)_{as}$
916 m	908(Bu)	20/0	916 m	905	907	22/0	907 (Bu)	23/0	916 m	913s	906	21/6	$\delta(CCN) + \nu(CC)$
	906(Bg)	0/18		902	904	0/28	904 (Bg)	0/31	906sh		906	21/6	$\delta(CCN) + \nu(CC)$
	846(Ag)	0/7		841	843	6/3	843 (Ag)	0/3	850 m	846s	840	25/2	$\nu(CS)_s + \delta(SCS) + \delta(CCH)$
854 m	846(Au)	32/0	848s	838	842	41/1	842 (Au)	50/0	843m		839	7/1	$\nu(CS)_s + \delta(SCS) + \delta(CCH)$
391s	378(Au)	126/0		355	375	65/5	364 (Ag)	0/16	400vs	392vs	390	76/0	$\nu(M-S)$
381w	368(Ag)	0/2	360s	351	367	47/7	362 (Au)	107/0			379	0/2	$\nu(M-S)$
	361(Bu)	2/0	327 m	314	321	2/0	315 (Au)	29/0	335 m	333 m	320	31/1	$\delta(CCN) + \nu(M-S)$
	331(Au)	1/0		312	319	17/0	311 (Ag)	0/4			314	0/2	$\delta(CCN) + \delta(SCN) + \nu(M-S)$

[a] Unscaled frequencies from periodic DFT calculations. [b] Asymmetrical bonding: Cu−S = 2.377, 2.330, 2.300, and 2.330 Å. [c] Symmetrical bonding: Cu−S = 2.359 Å. Au, Ag, Bu, and Bg represent the irreducible representations of the normal modes in C_{2h} molecular symmetry.

TABLE 8: Calculated Frequencies (Scaling Factor = 0.985), IR Intensity (I_{IR}), and Raman Activity (A_{Ra}) of AgMe$_2$dtc and AgEt$_2$dtc at the B3LYP/B2 Level and Comparison with the Experimental Raman Spectra

AgMe$_2$dtc							AgEt$_2$dtc			
unidentate		bidentate			expt (R_a)[50]		unidentate		bidentate	
frequency	I_{IR}/A_{Ra}	frequency	I_{IR}/I_{Ra}	assignment	10^{-6} (uni-)	10^{-5} (bi-)	frequency	I_{IR}/A_{Ra}	frequency	I_{IR}/A_{Ra}
1504	117/64	1513	158/3	$\delta(CH_3) + \nu(CN)$	1521 m	1514 m	1490	69/52	1504	107/20
1462	5/32	1465	26/22	$\delta(CH_3)$	1438w	1448 m	1471	9/18	1472	1/16
1377	132/154	1378	232/8	$\nu(CN) + \delta(CH_3)$	1386vs	1386vs	1425	112/82	1435	133/8
					1367sh					
1250	57/93	1274	64/3	$\nu(NC_R) + \delta(CH_3)$	1238vw		1210	51/87	1212	62/1
1133	94/138	1152	35/11	$\delta(CNC) + \delta(HCN)$	1148 m	1148s	1134	90/153	1148	66/8
1055	18/4	1054	23/0	$\delta(C_RNC)$	1035vw	1045 m	1063	20/4	1067	23/3
							1002	20/139	992	3/12
977	84/457	951	129/10	$\nu(C{=}S)$	933w	935w	968	41/203	962	54/7
				$\nu(C-S)_{as}$						
				$\delta(CCN) + \nu(CS)$			904	16/131	894	54/7
882	15/52	877	0/4	$\nu(C-S)_s + \nu(C_RN)$		850w	827	25/17	833	13/2
573	6/10	574	9/13	$\delta(C_RNC_R) + \nu(CS)$	559w	563 m	579	0/0	589	0/0
438	12/5	431	8/12	$\delta(CNC) + \delta(SCS)$	440vw	441 m	488	6/8	491	7/0
323	14/131	361	4/3	$\nu(M-S)$	340vw	340 m	337	4/48	378	2/7

ν_{as}(CS) vibrations. However, shoulders at 972 cm^{-1} for Ni(Et_2dtc)$_2$ and at 974 cm^{-1} for Cu(Et_2dtc)$_2$ are observed in the solid-state IR spectra of the complexes, and the origin of these shoulders is not clearly understood. It was previously accepted that splitting of the main ν_{as}(CS) absorption up to 20 cm^{-1} is indicative of asymmetrical dtc bonding.[47] However, it was further shown that due to the absence of a degenerate mode in the highest possible symmetry of the ligand bonding types (C_{2v}) no band splitting should be expected down to C_1 symmetry in the series $C_{2v}-C_2-C_s-C_1$, and hence the splittings observed come from interligand or intermolecular couplings.[48] For a better understanding of the observed shoulder of the main ν_{as}(CS) IR absorption peak in the solid state, we performed a series of calculations modeling in addition asymmetrical, uni- and bidentate bonding types. First, we simulated asymmetric bonding for Cu(Et_2dtc)$_2$, with different Cu−S bonds, and a planar CuS$_4$ fragment, and selected calculated frequencies are presented in Table 7. The calculated two components of ν_{as}(CS) absorption differ by up to 10 cm^{-1} in both C_{2h} (symmetrical bonding) and C_1 (asymmetrical bonding) structures of Cu(Et_2dtc)$_2$. The calculated IR intensities and Raman activities for the last case revealed that one of the vibrational modes is IR-active (991 cm^{-1}), and the second one is Raman-active (982 cm^{-1}). The same situation was predicted for the symmetrical bonding (all Cu−S bonds are equal, 2.359 Å), and therefore the splitting of ν_{as}(CS) absorption in the 1060−920 cm^{-1} region (if observed) could not be due to the asymmetrical M−S bonding as previously accepted by Bonati and Ugo.[47,48] Searching for a reliable explanation of the observed splitting, we performed additional geometry and frequency calculations simulating the asymmetrical bonding situation in the solid state with the nonplanar CuS$_4$ fragment as obtained from X-ray diffraction analysis. The solid-state structure simulation of Cu(Et_2dtc)$_2$ confirmed the splitting of the ν_{as}(CS) band; calculated frequencies are at 996 and 974 cm^{-1} (Table 7). The solid-state calculations revealed that due to the broken CuS$_4$ planarity the Raman-active ν_{as}(CS) component becomes also IR-active, and as a result a shoulder appears next to the main ν_{as}(CS) IR band. Hence, the splitting of the ν_{as}(CS) band (<20 cm^{-1}) in the 1060−920 cm^{-1} region (when observed) does not indicate M−S asymmetrical bonding in transition metal dtc complexes but rather the nonplanar CuS$_4$ fragment produced from intermolecular contacts in the solid state. In solution (CH$_2$Cl$_2$), the intermolecular contacts are not present, and the IR spectra of Ni(Et_2dtc)$_2$ and Cu(Et_2dtc)$_2$ complexes are in line with the enhanced complex symmetry and exhibit only one band in the

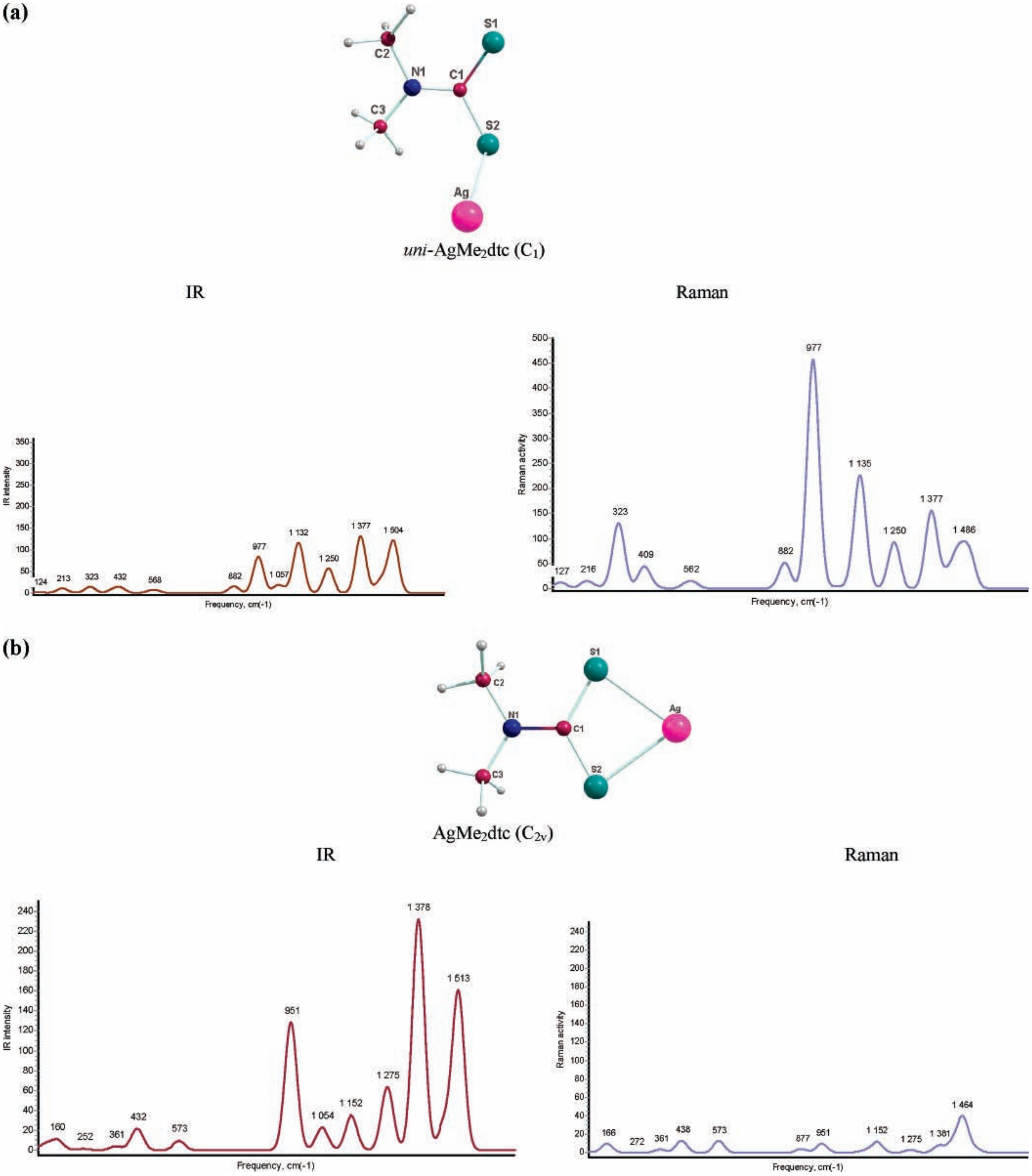

Figure 4. Optimized structures and calculated IR and Raman spectra of (a) unidentate AgMe$_2$dtc and (b) bidentate AgMe$_2$dtc.

ν_{as}(CS) region.[48] Such a vibrational behavior was predicted from our calculations of the isolated Ni(Et$_2$dtc)$_2$ and Cu(Et$_2$dtc)$_2$ complexes.

As already mentioned, in the relaxed Zn(Et$_2$dtc)$_2$ structure the angle A(S1−Zn−S2′) = 128°, and the symmetry leans toward tetrahedral, but the ultimate boundary case with A(S1−Zn−S4) = 109° is not achieved. The gas-phase frequency calculations at the optimized geometry of Zn(Et$_2$dtc)$_2$ revealed two IR-active ν_{as}(CS) vibrations at the same wavenumbers (982 cm^{-1}), and therefore only one band should appear in the IR spectrum of isolated Zn(Et$_2$dtc)$_2$. The prediction for the isolated Zn(Et$_2$dtc)$_2$ molecule is consistent with the solution spectrum pattern of Zn(Et$_2$dtc)$_2$ where intermolecular interactions are absent: One ν_{as}(CS) band is observed at 989 cm^{-1} (Table 7). In the solid-state spectrum, however, one band at 995 cm^{-1} and a pronounced shoulder at 983 cm^{-1} were observed. The presence of two bands in the ν_{as}(CS) region in the solid-state spectrum of Zn(Et$_2$dtc)$_2$ is explained by the presence of intermolecular

TABLE 9: Selected Calculated Frequencies (Scaling Factor = 0.985) and IR/Raman Intensities (in Brackets) of Me_2dtc, Me_2dtc^-, and $Cu(Me_2dtc)_2$ for Different Molecular Symmetries at the B3LYP/B1 Level of Theory

Me_2dtc	Me_2dtc^-	bidentate $Cu(Me_2dtc)_2$		unidentate $Cu(Me_2dtc)_2$	
C_1	C_1	D_{2h}	C_1	C_1	assignment
1517 (157)	1499 (14)	1523 A_g (0/4)	1537 (0/8)	1519 (123/278)	$\delta(CH_3) + \nu(CN)$
		1519 B_{3u} (705/0)	1534 (540/0)	1514 (702/77)	
1388 (216)	1333 (136)	1401 A_g (0/7)	1415 (0/33)	1397 (17/180)	$\nu(CN) + \delta(CH_3)$
		1396 B_{3u} (699/0)	1412 (416/0)	1392 (586/197)	
1010 (102)	972 (320)	990 B_{2u} (89/0)	979 (88/0)	962^a (20/867)	$\nu_{as}(CS)$
		978 B_{1g} (0/71)	967 (0/63)	960^a (16/4089)	$\nu_{as}(CS)$
913 (74)	886 (4/)	885 A_g (0/5)	901 (0/32)	874^b (6/144)	$\nu_s(CS) + \delta(SCS)$
		885 B_{3u} (2/0)	901 (1/0)	873^b (4/551)	$\nu_s(CS) + \delta(SCS)$
		351 A_g (0/7)	363 (0/11)	381 (3/3)	$\nu(CuS)$
		350 B_{3u} (117/0)	361 (122/0)	302 (0/160)	$\nu(CuS)$
		291 B_{2u} (2/0)	308 (2/0)		
		260 B_{1g} (0/7)	285 (0/14)		

[a] $\nu(C{=}S)$ [b] $\nu(C-S)$

coupling of the vibrational modes of the dimer $Zn(Et_2dtc)_2$ units (as obtained from X-ray diffraction analysis), producing non-degenerate frequencies for the two IR-active $\nu_{as}(CS)$ vibrations.[42]

The strong bands observed in the solid-state IR spectra of $Ni(Et_2dtc)_2$ at 854 cm^{-1}, of $Cu(Et_2dtc)_2$ at 848 cm^{-1}, and of $Zn(Et_2dtc)_2$ at 850 and 843 cm^{-1} are assigned to $\nu_s(CS)$ modes. As seen from Table 7, the vibrational behavior of $\nu_s(CS)$ modes for the complexes studied follows that of $\nu_{as}(CS)$ ones discussed above.

3.4.2. Vibrational Patterns of Uni- and Bidentate dtc Bonding in MR_2dtc (M = Ag(I) or Cu(II); R = Me or Et). First, the vibrational patterns of uni- and bidentate bonding of dtc were studied in a 1:1 model for AgR_2dtc complexes (R = Me or Et). The vibrational analysis was mainly focused on the positions and the IR intensities and Raman activities of $\nu(N-CS_2)$, $\nu_{as}(CS)$, $\nu_s(CS)$, and $\nu(AgS)$ frequencies as potential indicators of the bonding type of the dtc ligand. Selected calculated vibrational frequencies of the AgR_2dtc complexes are given in Table 8. Full vibrational analysis was performed, and the data are given in the Table 2S of the Supporting Information. The optimized structures and the calculated IR and Raman spectra of uni- and bidentate $AgMe_2dtc$ are given in Figure 4.

The $\nu(N-CS_2)$ frequency behavior in the M−dtc complexes was used previously (i) to predict the M−dtc bonding type (uni- or bidentate) and (ii) to trace the effect of the N-substituent on the M−L interaction strength: Higher $\nu(N-CS_2)$ frequencies of $M(Et_2dtc)$ in comparison with that of $M(Me_2dtc)$ have been related to stronger $M-Et_2dtc$ interactions.[49,50] We will show below that both correlations are doubtful. According to the model calculations for both uni- and bidentate bondings, the $\nu(N-CS_2)$ and $\delta(CH_3)$ modes remain strongly coupled, ruling out the possibility of finding correlation and estimating the ligand bonding type (the bands at 1504/1377 and 1490/1425 cm^{-1} for unidentate and 1513/1378 and 1504/1435 cm^{-1} for bidentate $AgMe_2dtc$ and $AgEt_2dtc$). The calculations predict that the $\nu(N-CS_2)$ vibrations of HMe_2dtc and HEt_2dtc should appear at 1388 and 1439 cm^{-1}, respectively. Obviously, the higher $\nu(N-CS_2)$ frequency (second one) of Et_2dtc could not originate from stronger $M-Et_2dtc$ interaction, as accepted previously; it is rather an intrinsic ligand property caused by the N-substituent (Me or Et). Hence, the position of the $\nu(N-CS_2)$ frequencies could not be used to distinguish the uni- and bidentate bonding types as well as to estimate the M−dtc interaction strength. Our calculations revealed, however, that the Raman activity of the $\nu(N-CS_2)$ band varies significantly going from uni- to bidentate AgR_2dtc bonding. For unidentate AgR_2dtc complexes, the Raman activity of the $\nu(N-CS_2)$ vibration is high, and it significantly decreases for the bidentate AgR_2dtc complexes. Therefore, the Raman activity of the $\nu(N-CS_2)$ frequency could be used to discern uni- and bidentate bonding in AgR_2dtc.

DFT frequency calculations of unidentate AgR_2dtc complexes predict the $\nu(C{=}S)$ and $\nu(C-S)$ vibrations to appear at 977/882 cm^{-1} for R = Me and at 968/827 cm^{-1} for R = Et (Table 8). Conversely to the common expectation, the lower $\nu(C{=}S)$ and higher $\nu(C-S)$ frequencies for $AgMe_2dtc$ than those for $AgEt_2dtc$ should mean stronger $Ag-S_2(Me_2dtc)$ bonding, in agreement with the predicted binding energies (Table 4). In the case of unidentate bonding in AgR_2dtc, the calculations suggest $\Delta(\nu_{C=S} - \nu_{C-S}) = 94$ cm^{-1} for R = Me and $\Delta(\nu_{C=S} - \nu_{C-S}) = 141$ cm^{-1} for R = Et. It should be noted that for $AgMe_2dtc$ the $\nu(C{=}S)$ and $\nu(C-S)$ frequencies are consecutive, whereas for $AgEt_2dtc$ the $\delta(CCN)$ vibration appears between the $\nu(C{=}S)$ and the $\nu(C-S)$ frequencies and makes an impression of $\nu(C{=}S)$ band splitting. A symmetrical bidentate bonding in AgR_2dtc produces $\nu_{as}(CS)$ and $\nu_s(CS)$ vibrations at 951 and 877 cm^{-1} for R = Me and at 962 and 833 cm^{-1} for R = Et (Table 8). As compared to the unidenate AgR_2dtc bonding, the bidentate one gives slightly smaller values of $\Delta(\nu_{as} - \nu_s) = 75$ cm^{-1} for R = Me and 129 cm^{-1} for R = Et. According to the calculations, the $\nu_{as}(CS)$ vibration is strong to medium in the IR spectrum and weak in the Raman spectrum, whereas the $\nu_s(CS)$ vibration is only Raman-active for R = Me and both IR- and Raman-active for R = Et. Like unidenate $AgEt_2dtc$, for bidentate $AgEt_2dtc$, the $\delta(CCN)$ vibration should appear between the $\nu_{as}(CS)$ and the $\nu_s(CS)$ vibrations (Table 8). In summary, our DFT vibrational analysis predicted one band due to the $\nu(C{=}S)$ of unidentate $AgMe_2dtc$ bonding or one due to the $\nu_{as}(CS)$ of bidentate $AgMe_2dtc$ bonding in the 1060−920 cm^{-1} region; the $\nu(C{=}S)$ frequency is upshifted by 6−27 cm^{-1} than $\nu_{as}(CS)$ one. Therefore, the number of the bands in this region is not indicative of uni- or bidentate bonding in AgR_2dtc. In the 900−800 cm^{-1} region, one $\nu(CS)$ band for uni- or one $\nu_s(CS)$ band for bidentate AgR_2dtc is expected at nearby positions.

The calculations suggested further that important vibrational characteristic that can be used to discern uni- and bidentate bonding in the 1060−920 cm^{-1} region is the Raman activity of the $\nu(CS)$ band: It is very high for the unidentate AgR_2dtc bonding ($\nu(C{=}S)$ vibration) and low for the bidentate AgR_2dtc bonding ($\nu_{as}(CS)$) (Figure 4). Therefore, Raman and surface-enhanced Raman spectroscopy have been applied successfully to distinguish uni- and bidentate geometries of ziram on a silver surface.[51] It should be mentioned that the Raman activity of the bands due to the bending HCN and CNC vibrations in the 1130−1150 cm^{-1} region is also significant for unidentate complexes and strongly decreases in bidentate ones (Figure 4).

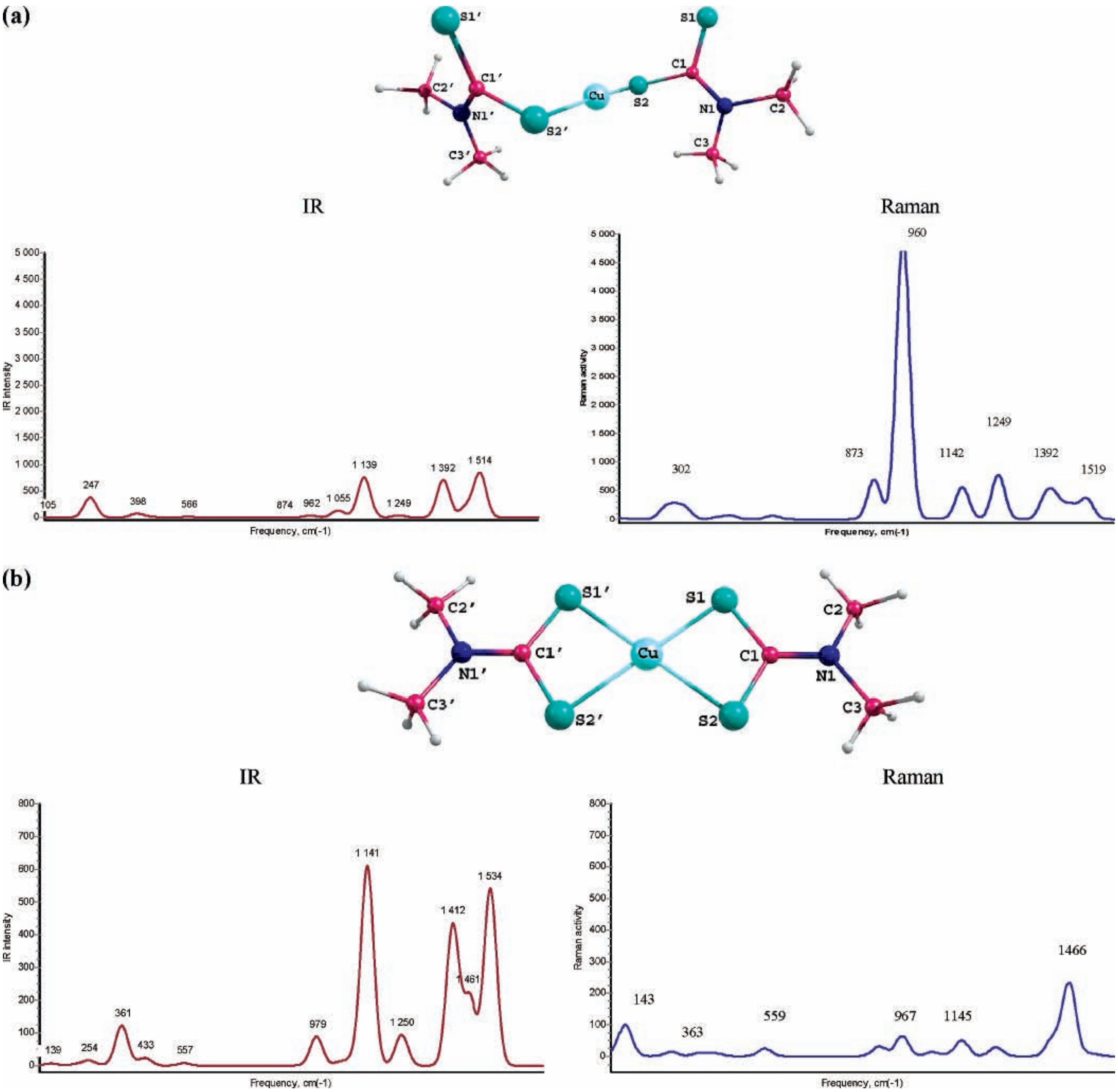

Figure 5. Optimized structures and calculated IR and Raman spectra of (a) unidentate Cu(Me$_2$dtc)$_2$ and (b) bidentate Cu(Me$_2$dtc)$_2$.

The ν(AgS) frequencies of unidentate AgR$_2$dtc complexes, calculated at 323 cm^{-1} (R = Me) and 337 cm^{-1} (R = Et), are at lower frequencies than those of bidentate AgR$_2$dtc complexes (361 cm^{-1} (R = Me) and 378 cm^{-1} (R = Et)). The IR intensity of ν(AgS) is low. However, high Raman activity of the ν(AgS) frequency for unidentate bonding and low Raman activity for bidenate AgR$_2$dtc bonding are found (Figure 4). Hence, the ν(AgS) frequency and its Raman activity can also be used as indicators of the dtc bonding type in the metal complexes.

Further, the vibrational behavior of uni- and bidentate bonding of R$_2$dtc is studied for Cu(II) dtc complexes, using Cu(Me$_2$dtc)$_2$ in the Cu/Me$_2$dtc = 1:2 ratio. The calculated ν(N−CS$_2$), ν(CS), and ν(CuS) frequencies of Me$_2$dtc, Me$_2$dtc$^-$, and Cu(Me$_2$dtc)$_2$ are presented in Table 9. The calculated IR and Raman spectra of uni- and bidentate Cu(Me$_2$dtc)$_2$ are given in Figure 5. To estimate the effect of molecular symmetry on the vibrational pattern, the vibrational calculations are performed for bidentate bis-Cu(Me$_2$dtc)$_2$ in the highest D_{2h} and lowest C_1 symmetries. The bidentate Cu(Me$_2$dtc)$_2$ complex in D_{2h} and C_1 symmetries reveals a planar S−C−N−C fragment. The more stable C_1 structure (by 1 kcal/mol) is a minimum, and it differs from the D_{2h} structure by the asymmetrical location of the CH$_3$ groups. In that case, the bidentate Cu(Me$_2$dtc)$_2$ bondings in D_{2h} and C_1 symmetries revealed the same trend of ν(N−CS$_2$), ν(CS), and ν(CuS) frequencies and intensities. On passing from Me$_2$dtc and Me$_2$dtc$^-$ to the bidenate Cu(Me$_2$dtc)$_2$ bonding, the ν(N−CS$_2$) frequency is blue-shifted, indicating an increase of the carbon−nitrogen double bond character. Because the Cu(Me$_2$dtc)$_2$ complex consists of two ligands, pairs of ν(N−CS$_2$), ν(CS)$_{as}$, ν(CS)$_s$, and ν(CuS) frequencies are suggested from the calculations. The bidentate bonding reveals that for each pair one frequency is IR-active, and other one is Raman-active. Hence, in the IR spectrum of bidentate Cu(Me$_2$dtc)$_2$, one narrow ν(N−CS$_2$) (1534 or 1412 cm^{-1}), one ν_{as}(CS) (979 cm^{-1}), and one ν(CuS) (361 cm^{-1}) band should appear (Figure 5). Due to the low IR and Raman intensities, the ν_s(CS) band is not indicative. Generally, the frequencies of the bidentate $Cu(Me_2dtc)_2$ show low Raman activity. The unidentate bonding produces two almost degenerate frequencies with IR and Raman activities for each vibration. Hence, broad bands for $\nu(N-CS_2)$, $\nu(C{=}S)$, and $\nu(C-S)$ modes of unidenate $Cu(Me_2dtc)_2$ are expected. In contrast to the low Raman activity for the bidentate bonding, $\nu(N-CS_2)$ ($\nu(C{=}S)$ (962 cm^{-1}), $\nu(C-S)$ (875 cm^{-1}), and $\nu(Cu-S)$ (302 cm^{-1}) show high Raman activity (Table 9 and Figure 5). Therefore, the vibrational study of uni- and bidentate $Cu(Me_2dtc)_2$ complexes confirmed the trends obtained for uni- and bidentate $AgMe_2dtc$: high Raman activities for $\nu(N-CS_2)$, $\nu(CS)$, and $\nu(CuS)$ bands in the case of unidentate bonding and low Raman activities in the case of bidentate bonding. The calculated spectra of uni- and bidenate complexes reveal similar values of $\Delta(\nu_{c=s} - \nu_{c-s} / \nu_{as} - \nu_s) = 70-80$ cm^{-1}.

The comparison of the vibrational behavior of the $\nu(N-CS_2)$, $\nu(CS)$, and $\nu(CuS)$ modes of the bidentate $Cu(Et_2dtc)_2$ complex to those of the $Cu(Me_2dtc)_2$ complex showed only one exception: The band next to the $\nu_{as}(CS)$ band (which should appear at ~900 cm^{-1}) is attributed to the $\nu_s(CS)$ vibration for $Cu(Me_2dtc)_2$ and to the $\delta(CCN)$ vibrations for $Cu(Et_2dtc)_2$. The $\nu_s(CS)$ vibrations of $Cu(Et_2dtc)_2$ appear at a lower frequency, 840 cm^{-1}; hence, the frequency difference ($\Delta(\nu_s - \nu_{as})$) of $Cu(Et_2dtc)_2$ is larger (~150 cm^{-1}) than that of the $Cu(Me_2dtc)_2$ complex (~50 cm^{-1}).

4. Conclusions

The reliability of the DFT/B3LYP method (with 6-31++G(d,p) for the ligand atoms and 6-311+G(d) for Ni(II), Cu(II), and Zn(II) ions) to predict the geometrical parameters and spin state of metal complexes of R_2dtc (R = H, Me, or Et) is verified by virtue of available experimental geometries. Gas-phase optimization of $Cu(Et_2dtc)_2$ reveals symmetrical M−S bonding, whereas the periodic DFT calculations (including unit cell parameters) lead to asymmetrical M−S bonding in agreement with the experiment. The results obtained showed more complicated correlations for $M(II)-R_2dtc$ bonding in $M(R_2dtc)_2$ complexes than $M(R_2dtc)^+$ ones. According to the EPA calculations, the electrostatic attraction is the dominant contribution to the $M-S_2(R_2dtc)$ bonding. The orders of the electrostatic attractions and the orbital interactions follow the trend of the total binding energy, revealing that both contributions are responsible for the binding energy order. The calculated M−L binding energy decreases in the order $Ni-S_2$ ($Ni(R_2dtc)_2$) > $Zn-S_2$ ($Zn(R_2dtc)_2$) > $Ag-S_2$ (AgR_2dtc) > $Cu-S_2$ ($Cu(R_2dtc)_2$). The calculated π-back-donation is very small, and the σ-donation is the dominant contribution to the donor−acceptor interaction in $Ni(R_2dtc)_2$, $Cu(R_2dtc)_2$, and $Zn(R_2dtc)_2$ complexes.

The calculated formation reaction energies of $M(R_2dtc)_2$ complexes in the gas phase and solution showed (i) a decrease of the stability in the order $Ni(R_2dtc)_2 > Cu(R_2dtc)_2 > Zn(R_2dtc)_2$, (ii) a slightly larger stabilization of $M(Et_2dtc)_2$ complexes than that of $M(Me_2dtc)_2$, and (iii) a stabilization of $M(II)(R_2dtc)_2$ complexes going from the gas phase (nonpolar solvent) to a polar solvent and destabilization of the bidentate AgR_2dtc in a polar solution. The calculated formation reaction energies are in agreement with available experimental data. According to the calculations in solution, Ni(II) is the metal that most likely should inhibit the transformation reaction of dtc in soil followed by Cu(II), Zn(II), and Ag(I).

The results from the theoretical (DFT) vibrational study of uni- and bidenate bonding in R_2dtc metal complexes for the $M(I)/R_2dtc$ ratio = 1:1 (AgR_2dtc) and for the $M(II)/R_2dtc$ ratio = 1:2 ($Cu(R_2dtc)_2$) showed the following trends: (i) For uni- and bidentate bondings in AgR_2dtc complexes, one band in the 1060−920 cm^{-1} IR/Raman region is expected (due to $\nu(C{=}S)$ and $\nu_{as}(C-S)$ vibrations, respectively), (ii) for the unidentate $Cu(Me_2dtc)_2$ complex, both $\nu(C{=}S)$ frequencies are degenerate, both are IR- and Raman-active, and therefore one broad $\nu(C{=}S)$ band should appear, and (iii) for bidentate $Cu(R_2dtc)_2$ one $\nu_{as}(CS)$ band is IR-active, the other one is Raman-active ($\Delta \approx$ 10 cm^{-1}), and hence a shoulder of the main $\nu_{as}(CS)$ band is expected to appear when the symmetry lowers. The number of bands in the 1060−920 cm^{-1} region is not indicative of the $M-R_2dtc$ bonding type because one band is predicted for both uni- and bidentate bonding of dtc as well as for symmetrical and asymmetrical M−S bondings. Periodic frequency calculations for $Cu(Et_2dtc)_2$ showed that splitting of the main $\nu_{as}(CS)$ band is an indication of the nonplanar MS_4 fragment due to the intermolecular couplings.

Uni- and bidentate $AgMe_2dtc$ and $Cu(Me_2dtc)_2$ complexes produce a similar splitting of the $\nu(CS)$ band $\Delta(\nu_{C=S} - \nu_{C-S}/\nu_{as} - \nu_s) = 70-90$ cm^{-1}, whereas uni- and bidentate $AgEt_2dtc$ and $Cu(Et_2dtc)_2$ complexes give a larger splitting of the $\nu(CS)$ band $\Delta(\nu_{C=S} - \nu_{C-S}/\nu_{as} - \nu_s) = 120-140$ cm^{-1}. In the case of metal complexes of Et_2dtc, the $\nu(C{=}S)$ and $\nu(C-S)$ as well as $\nu_{as}(CS)$ and $\nu_s(CS)$ frequencies are not consecutive; the $\delta(CCN)$ vibration appears between them and makes an impression of splitting of the $\nu(CS)$ band.

The most important vibrational characteristic that can be used to discern uni- and bidentate bonding of AgR_2dtc and $Cu(R_2dtc)_2$ complexes is the Raman activity of the $\nu_{as}(CS)$ ($\nu(C{=}S)$) band in the 1060−920 cm^{-1} region: It is very high for the unidentate bonding and low for the bidentate bonding. A similar trend is observed for $\nu(N-CS_2)$, $\nu_s(CS)$, and $\nu(MS)$ bands, and they also could be applied as indicators of the $M-R_2dtc$ bonding type.

Acknowledgment. The authors are grateful to the reviewer for the constructive recommendations that improved the quality of the paper.

Supporting Information Available: Full list of experimental and calculated vibrational spectra of $Ni(Et_2dtc)_2$, $Cu(Et_2dtc)_2$, and $Zn(Et_2dtc)_2$ at the B3LYP/B1 level and calculated vibrational spectra of $Ag(Me_2dtc)$ and $Ag(Et_2dtc)$ at the B3LYP/B2 level. This material is available free of charge via the Internet at http://pubs.acs.org.

References and Notes

(1) Sachinidis, J.; Grant, M. W. *Aust. J. Chem.* **1981**, *34*, 2195.

(2) Ribeiro da Silva, M. A. V.; Reis, A. M. M. V.; Ferreira da Silva, M. M. R. *J. Chem. Thermodyn.* **2000**, *32*, 1319.

(3) Ribeiro da Silva, M. A. V.; Reis, A. M. M. V.; Faria, R. I. M. C. P. *J. Chem. Thermodyn.* **1995**, *27*, 1365.

(4) Porento, M.; Hirva, P. *Theor. Chem. Acc.* **2002**, *107*, 200.

(5) Yang, Y.; Zuo, B.; Li, J.; Chen, G. *Spectrochim. Acta, Part A* **1996**, *52*, 1915.

(6) Lee, C.-R.; Tan, L.-Y.; Wang, Y. *J. Phys. Chem. Solids* **2001**, *62*, 1613.

(7) (a) Thorn, G. D.; Ludwig, R. A. *The Dithiocarbamates and Related Compounds*; Elsevier Publishing Company: Amsterdam, 1962. (b) Jankiewicz, B.; Ptaszyński, B.; Turek, A. *Pol. J. Environ. Stud.* **1999**, *8*, 35.

(8) Magee, R. J. *Rev. Anal. Chem.* **1973**, *1*, 335.

(9) Sawhney, B. L.; Brown, K. *Soil Sci. Soc. Am.* **1989** (Special Publication No. 22, Madison, WI).

(10) (a) West, R.; Sunderman, F. W. *Am. J. Med. Soc.* **1929**, *50*, 3106. (b) Viola-Rhenals, M.; Rieber, M. S.; Rieber, M. *Biochem. Pharmacol.* **2006**, *71*, 722.

(11) . McCleverty, J. A.; Morrison, N. J.; Spencer, N.; Ashworth, C. C.; Bailey, N. A.; Johnson, M. R.; Smith, J. M. A.; Tabbiner, B. A.; Taylor, C. R. *J. Chem. Soc., Dalton Trans.* **1980**, 1945.

(12) Matolcsy, G.; Nadasy, M.; Andriska, V. *Pestic. Chem.: Studies in Environmental Science*; Elsevier; **1988**, *32*, 503.

(13) Matlock, M. M.; Henke, K. R.; Atwood, D. A. *J. Hazard. Mater.* **2002**, *92*, 129.

(14) Ünlü, N.; Ersoz, M. *Sep. Purif. Technol.* **2007**, *52*, 461.

(15) Andrus, M. E. *Met. Finish.* **2000**, *11*, 20.

(16) Li, Y. J.; Zeng, X. P.; Liu, Y. F.; Yan, S. S. *Sep. Purif. Technol.* **2003**, *31*, 91.

(17) Miertus, S.; Scrocco, E.; Tomasi, J. *Chem. Phys.* **1981**, *55*, 117.

(18) Miertus, S.; Tomasi, J. *Chem. Phys.* **1982**, *65*, 239.

(19) Cossi, M.; Barone, V.; Cammi, R.; Tomasi, J. *Chem. Phys. Lett.* **1996**, *255*, 327.

(20) Lee, C.; Yang, W.; Parr, R. G. *Phys. Rev. B* **1988**, *37*, 785.

(21) Lee, C.; Yang, W.; Parr, R. G. *Phys. Rev. B* **1988**, *33*, 3098.

(22) Becke, A. D. *J. Chem. Phys.* **1993**, *98*, 5648.

(23) Becke, A. D. *J. Chem. Phys.* **1993**, *98*, 1372.

(24) Head-Gordon, M.; Head-Gordon, T. *Chem. Phys. Lett.* **1994**, *220*, 122.

(25) Scuseria, G. E.; Schaefer, H. F., III. *J. Chem. Phys.* **1989**, *90*, 3700.

(26) Georgieva, I.; Trendafilova, N.; Rodriguez-Santiago, L.; Sodupe, M. *J. Phys. Chem. A* **2005**, *109*, 5668.

(27) Frisch, M. J.; Trucks, G. W.; Schlegel, H. B.; Scuseria, G. E.; Robb, M. A.; Cheeseman, J. R.; Montgomery, J. A., Jr.; Vreven, T.; Kudin, K. N.; Burant, J. C.; Millam, J. M.; Iyengar, S. S.; Tomasi, J.; Barone, V.; Mennucci, B.; Cossi, M.; Scalmani, G.; Rega, N.; Petersson, G. A.; Nakatsuji, H.; Hada, M.; Ehara, M.; Toyota, K.; Fukuda, R.; Hasegawa, J.; Ishida, M.; Nakajima, T.; Honda, Y.; Kitao, O.; Nakai, H.; Klene, M.; Li, X.; Knox, J. E.; Hratchian, H. P.; Cross, J. B.; Bakken, V.; Adamo, C.; Jaramillo, J.; Gomperts, R.; Stratmann, R. E.; Yazyev, O.; Austin, A. J.; Cammi, R.; Pomelli, C.; Ochterski, J. W.; Ayala, P. Y.; Morokuma, K.; Voth, G. A.; Salvador, P.; Dannenberg, J. J.; Zakrzewski, V. G.; Dapprich, S.; Daniels, A. D.; Strain, M. C.; Farkas, O.; Malick, D. K.; Rabuck, A. D.; Raghavachari, K.; Foresman, J. B.; Ortiz, J. V.; Cui, Q.; Baboul, A. G.; Clifford, S.; Cioslowski, J.; Stefanov, B. B.; Liu, G.; Liashenko, A.; Piskorz, P.; Komaromi, I.; Martin, R. L.; Fox, D. J.; Keith, T.; Al-Laham, M. A.; Peng, C. Y.; Nanayakkara, A.; Challacombe, M.; Gill, P. M. W.; Johnson, B.; Chen, W.; Wong, M. W.; Gonzalez, C.; Pople, J. A. *Gaussian 03*, revision B.05; Gaussian, Inc.: Wallingford, CT, 2004.

(28) (a) Reed, A. E.; Curtiss, L. A.; Weinhold, F. *Chem. Rev.* **1988**, *88*, 899. (b) Hirshfeld, F. L. *Theor. Chim. Acta* **1977**, *44*, 129.

(29) (a) Xantheas, S. S. *J. Chem. Phys.* **1996**, *104*, 8821. (b) Boys, S. F.; Bernardi, F. *Mol. Phys.* **1970**, *19*, 553. (c) van Duijneveldt, F. B.; van Duijneveldt-van de Rijdt, J. G. C. M.; van Lenthe, J. H. *Chem. Rev.* **1994**, *94*, 1873. (d) Valiron, P.; Mayer, I. *Chem. Phys. Lett.* **1997**, *275*, 46.

(30) Morokuma, K. *J. Chem. Phys.* **1971**, *55*, 1236.

(31) Ziegler, T.; Rauk, A. *Theor. Chim. Acta* **1977**, *46*, 1.

(32) te Velde, G.; Bickelhaupt, F. M.; Baerends, E. J.; Fonseca Guerra, C.; van Gisbergen, S. J. A.; Snijders, J. G.; Ziegler, T. *J. Comput. Chem.* **2001**, *22*, 931.

(33) Perdew, J. P.; Chevary, J. A.; Vosko, S. H.; Jackson, K. A.; Pederson, M. R.; Singh, D. J.; Fiolhais, C. *Phys. Rev. B* **1992**, *46*, 6671.

(34) (a) van Lenthe, E.; Baerends, E. J.; Snijders, J. G. *J. Chem. Phys.* **1993**, *99*, 4597. (b) van Lenthe, E.; Baerends, E. J.; Snijders, J. G. *J. Chem. Phys.* **1994**, *101*, 9783. (c) van Lenthe, E.; Ehlers, A. E.; Baerends, E. J. *J. Chem. Phys.* **1999**, *110*, 8943.

(35) van Lenthe, E.; van Leeuwen, R.; Baerends, E. J.; Snijders, J. G. *Int. J. Quantum Chem.* **1996**, *57*, 281.

(36) (a) Dapprich, S.; Frenking, G. *J. Phys. Chem.* **1995**, *99*, 93. (b) Frenking, G.; Pidun, U. *J. Chem. Soc., Dalton Trans.* **1997**, 1653. (c) The CDA calculations were carried out with the program CDA: Dapprich, S.; Frenking, G. *CDA*; Phillips-Universität Marburg: Marburg, Germany, 1994.

(37) Decker, S. A.; Klobukowski, M. *J. Am. Chem. Soc.* **1998**, *120*, 9342.

(38) (a) Kresse, G.; Hafner, J. *Phys. Rev. B* **1993**, *47*, RC558. (b) Kresse, G. Thesis, Technische Universität Wien, Vienna, Austria, 1993. (c) Kresse, G.; Furthmüller, J. *Comput. Mater. Sci.* **1996**, *6*, 15. (d) Kresse, G.; Furthmüller, J. *Phys. Rev. B* **1996**, *54*, 11169.

(39) Bonamico, M.; Dessy, G.; Mariani, C.; Vaciago, A.; Zambonelli, L. *Acta Crystallogr.* **1965**, *19*, 619.

(40) Bonamico, M.; Dessy, G.; Mugnoli, A.; Vaciago, A.; Zambonelli, L. *Acta Crystallogr.* **1965**, *19*, 886.

(41) Bonamico, M.; Mazzonet, G.; Vaciago, A.; Zambonelli, L. *Acta Crystallogr.* **1965**, *19*, 898.

(42) (a) Trendafilova, N.; Kellner, R. *Spectrochim. Acta* **1991**, *47*, 1559. (b) Kellner, R.; Gidaly, G.; Nikolov, G. St.; Trendafilova, N. S. *Mikrochim. Acta* **1983**, 183.

(43) Guerra, C. F.; Handgraaf, J.-W.; Baerends, E. J.; Bickelhaupt, F. M. *J. Comput. Chem.* **2004**, *25*, 189.

(44) Ribeiro da Silva, M. A. V.; Reis, A. M. M. V. *J. Chem. Thermodyn.* **1989**, *21*, 423.

(45) Ribeiro da Silva, M. A. V.; Reis, A. M. M. V. *J. Chem. Thermodyn.* **1989**, *21*, 167.

(46) Dietz, O.; Rayón, V. M.; Frenking, G. *Inorg. Chem.* **2003**, *42*, 4977.

(47) Bonati, F.; Ugo, R. J. *Organomet. Chem.* **1967**, *10*, 257.

(48) Kelner, R.; Nikolov, G. St.; Trendafilova, N. *Inorg. Chim. Acta* **1984**, *84*, 233.

(49) Herlinger, A. W.; Wenhold, S. N.; Long, T. V. *J. Am. Chem. Soc.* **1970**, *92*, 6474.

(50) (a) Brown, D. A.; Glass, W. K.; Burke, M. A. *Spectrochim. Acta* **1976**, *32*, 137. (b) Frigerio, A.; Halac, B.; Perec, M. *Inorg. Chim. Acta* **1989**, *1564*, 149.

(51) Sánchez-Cortés, S.; Vasina, M.; Francioso, O.; García-Ramos, J. V. *Vib. Spectrosc.* **1998**, *17*, 133.